SURFACE RECONSTRUCTION AND CHANGE DETECTION FOR AGRICULTURAL PURPOSES BY CLOSE RANGE PHOTOGRAMMETRY

Katharina Helming[Δ], Wolfgang Jeschke[¶], Juergen Storl
Technical University of Berlin, EB 9
Germany

Commission V

[Δ]now at Zentrum f. Agrarlandschafts- und Landnutzungsforschung, Müncheberg
[¶] now with Siemens Nixdorf Information Systems (SNI), Munich

ABSTRACT:

From 1987 through 1991 a so-called *Interdisciplinary Research Project* had been carried out at the TU Berlin. This project brought together scientists from various disciplines, i.e. photogrammetrists, soil scientists, geologists, and material research scientists. Their common aim was to develop working solutions for registration, numerical evaluation, and interpretation of surfaces from close-range photogrammetry and Raster Electron Microscopy (REM). The photogrammetric task within this project was to provide Digital Elevation Models (DEMs) of a representative selection of typical surfaces that were to be evaluated for their information content by the project partners. This paper reports on analog (and digital) data acquisition, photogrammetric processing, DEM determination and interpretation, and conclusions of the joint work of photogrammetric and water-agricultural scientists. The microrelief of soil before, during, and after more or less heavy rain had to be defined by photogrammetric methods. Knowing this relief, the amounts of rain, and the related infiltration and draining rates it should be possible to give recommendations for an erosion minimizing treatment of soil.

KEYWORDS: Close-range, DEM, Image Matching, Soil Erosion, Stereoscopic, Surface Measurement

INTRODUCTION

Soil erosion problem

Soil erosion due to water impact is an agricultural and – increasingly – an ecological problem since fertile soil is washed away from the fields and, likewise, nutrients and pesticides are flushed to the outflows. In order to fight the causes of erosion a detailed knowledge of the erosion process – and its releasing factors as well – is essential. Erosion most frequently starts on bare soil where rain energy leads to a silt of the upper soil layer, thus hindering infiltration and supporting runoff instead. The so-called *splash process* that is induced by the raindrop impact force results in a sealed surface. Any raindrop hitting the ground causes development of a crater on the soil surface where the vertical forces of the drop are transformed into radial forces. When reaching maximum height, the crest of a crater ejects little droplets consisting of water and small soil particles (Ferreira & Singer 1985). These particles are able to tamp the draining pores and to form with their layer-like deposit an infiltration-hampering seal.

This *interrill erosion* is a rain energy driven process which is strongly influenced by surface conditions and structures. Leaving out the plants covering the ground it is the *microrelief* of the surface that plays the most important role in this process since it has a decisive influence on the formation of the surface. Microrelief is the definition for the relief range from 2 mm up to 200 mm that is formed by secondary tillage. It is non-directional and is characterized by aggregates and clods (Römkens & Wang 1984). Much work has been done to analyze its important influence on erosion and to prove that an increase in surface *roughness* will enhance infiltration and lead to a decrease in runoff (Johnson et al. 1979, Steichen 1984). Possible reasons are:

- the rougher a microrelief, the lower is the frequency of raindrop impact with reference to surface area and time as well as its effective angle. This leads to a decline of the sealing process (Linden et al. 1988) – i.e. this process is not controlled by the kinetic energy of the rainfall. It is just its effective (i.e. normal) component that causes interrill erosion.
- a rougher microrelief leads to a higher *depressional storage*, thus delaying the runoff begin (Moore & Larson 1979).

Measurement efforts

Up to now no exact quantitative evaluation has been possible, since scientists were lacking methods for the precise measurement of the microrelief (elevation measures for the surface are needed that are collected with a spacing of less than 2 mm and have a height precision of 0.2 mm or better). Moreover, the measurements have to be restricted to contact-free methods in order to permit multitemporal surveys (e.g. linked to artificial rain tests) of a surface.

There have been some relief measurements over the last 40 years. First generation mechanical relief meters consisted of a board with moving steel needles (Burwell et al. 1963) which vertical position could be measured. Spacing used was from 50 mm to 100 mm. Further development of this technique resulted in automation (i.e. photographic or electronic registration) and a spacing scaled down to 5 mm (Currence & Lovely 1970, Moore & Larson 1979, Tessier et al. 1989). This spacing and, more important, the vertical resolution of more than 1 mm still hindered detailed evaluations and, in

particular, left 'footprints' on the ground that made multitemporal work impossible. Recently, tools with optical sensors have been developed to provide fast, high-resolution, contact-free measurements. These systems work on a photogrammetric basis (Ullah & Dickinson 1979) or rely on laser point triangulation (Huang & Bradford 1990a). Both methods are able to meet the requirements for a detailed physical interpretation of surfaces.

The aim of this investigation was to quantify the causal factors by which the microrelief influences interrill erosion and to register the effect on surface runoff. Comprehensive tests were performed in order to do this. In a rain simulator soil probes with different microreliefs were rained on. Each relief was evaluated before and after the rain, respectively. Further tests took place on outdoor fields to prove the universality of the results determined in the laboratory. From the photogrammetrically measured *Digital Elevation Models* (DEMs) indices for each surface are derived as well as spatial microrelief structures are exposed by geostatistical processing. Furthermore, deterministic models are developed that permit a quantitative evaluation of the depression reservoir capacity and the effective rain energy as derived from the microrelief. This allows to verify the above mentioned theories.

TEST SERIES

The rainfall simulator used in the laboratory had a drop size distribution equal to natural rainfall. It provides variable rainfall intensity and rain energy matches about 95% of the energy of similar natural rain. For a detailed description of the system see Roth & Helming (1992). In this simulator an Ap-horizon soil of a Haplic Luvisol derived from loess (5% slope) was irrigated for two hours with an 30 mm/h intensity (figs. 1a, 1b). Different kinds of microrelief were produced by passing the soil through a sieve. Three constellations were evaluated, i.e.

- rough (r); 50 mm sieve; seedbed for winter wheat
- medium (m); 25 mm sieve; seedbed for sugar beet
- fine (f); 10 mm sieve; seedbed for rape

Surface runoff was measured every two minutes. Before and after raining the microrelief was measured on a 0.2 m^2 area within the 1 m^2 area that was rained on. DEM spacing was 2 mm, yielding 50,000 points.

For open air verification tests were done on two sugar beet fields in Lower Saxony, Germany. The soil was a Haplic Luvisol too. Measurements on a 0.98 m^2 area with 3 mm horizontal spacing were performed just after seeding (March/April) and four months later at the end of July, respectively.

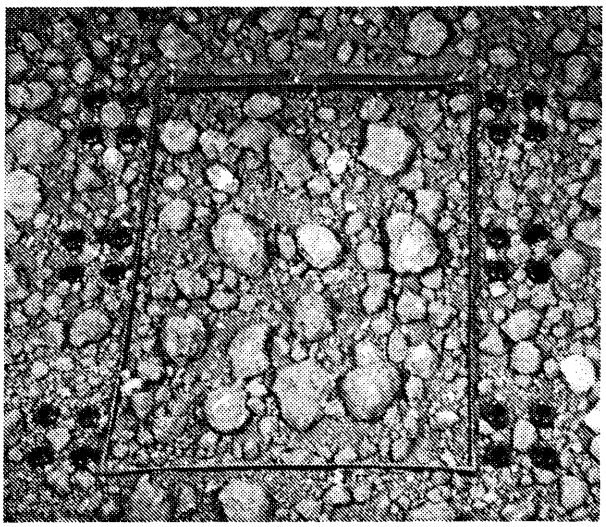

Fig. 1a: Soil test surface before rain

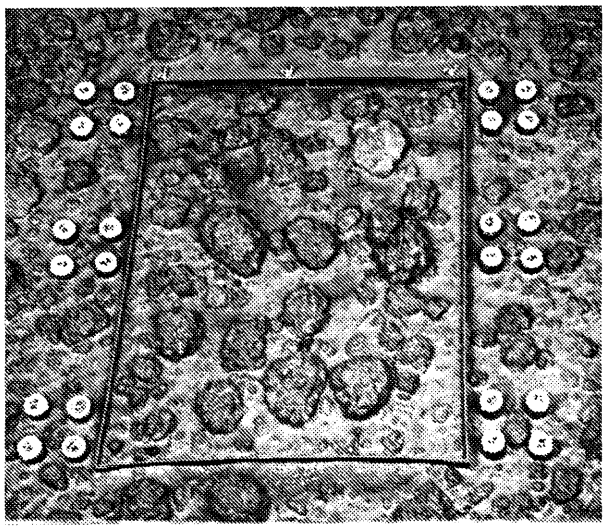

Fig. 1b: Same test site after 60 mm rain

IMAGE ACQUISITION

Analog Images

Choice of a suitable image acquisition configuration depends on requirements relating to the accuracy finally wanted and on limitations due to the object environment. In this project the objective was measurement of rectangular areas (1 x 1 m^2 in the field, 0.4 x 0.5 m^2 in the laboratory rain simulator tests) in order to connect quantitatively rain with erosion, i.e. to register changes in soil relief. For change detection normally three epochs were used, evaluating the soil relief before and after different rain periods. The periods between image acquisition dates in the laboratory, where intensity and duration of the rain could be controlled and measured accurately, were easily predefined since the simulated rain could be interrupted at any time, e.g. after 30 minutes, to have a break of some 10 minutes for

image acquisition, and then be continued. However, during field measurements image acquisition was dated at short notice, depending on the amount of rainfall since the last photograph. Ideally, images are captured immediately after heavy rainfall that could have a measureable effect on the soil relief. Portable equipment is needed because field test sites often are not accessible to cars.

Providing DEMs of the soil test areas (2 or 3 mm grid spacing, height accuracy better than 0.5 mm) was the photogrammetric task. Test areas were enclosed by rectangular metal frames which collected all sheet wash and such allowed to measure the quantity of water that caused the erosion. Since the coordinate system could be chosen freely – as only relative heights were of importance – the corners of these frames could be used as reference points, measuring their relative heights by nivellement. Thus exact surface slope angles could easily be obtained – a parameter that directly influences overland flow. Installing a sufficient number of reference points in the field proved to be nearly impossible, as test areas lay on farming land with no stable ground. Considering these circumstances the stereometric camera Zeiss SMK 40 was chosen for this project, a conventional close-range photogrammetric camera that is well known for its good image quality if calibrated thoroughly. An important point was the simple constellation for image acquisition where no control points were needed due to the cameras fixed relative orientation and stable calibration. The projected accuracy, which was better than 0.5 mm in all three dimensions, in connection with an object area of 1 m^2 (field measurement) resp. 0.2 m^2 (laboratory) could be met by this camera type using close-range lenses with a focal distance of about 1.5 m.

After developing the glass plates and reproducing the photographs on paper positives (or on film transparencies, depending on the scanner), scanning was done with a resolution of 20 µm per pixel, corresponding to 0.4 mm in object space ground coordinates. Digital images covering the area of interest were about 1,500 x 1,500 pixels wide in the case of the laboratory measurements and 2,500 x 2,500 pixels for field measurements. The image acquisition process for any series of about 60 exposed glass plates, including plate development and scanning, took between one and two weeks until the material was ready for digital image evaluation. While two people are needed for the image acquisition itself thanks to material transport requirements – especially for the weighty SMK camera and tripod – preparations, development, and scanning could be done by one person only, a method that proved to be practicable. Meanwhile, products for scanning of analog photographs have entered the photogrammetry-oriented production lines of manufacturers – the Zeiss PS1 photogrammetric scanner recently was developed right for this task.

There are certain drawbacks of this rather traditional way. First, bulky equipment has to be carried. Then, the number of possible images for a project is limited, since photographic plates have to be inserted into their cassettes in a dark room. Moreover, image evaluation may start only days later due to the lengthy photographic process, so there is no immediate control for image quality.

Digital Images

But these limitations can be overcome by using direct digital image acquisition. Immediate image control, e.g. checking image geometry and radiometry or correlation fitness, is at hand. Plates and film are replaced by magnetical and optical storage media, thus permitting a virtually unlimited registration capacity. The equipment for digital image acquisition, if still of considerable bulk and weight, is considerably easier to handle than the SMK 40. The cameras themselves are small and light, no large tripods have to be carried around. The heaviest parts are the batteries for the field power supply.

When there are so many advantages of digital cameras, why did we not use them in this project? The one simple reason is, that at project start there were none on the market that met the accuracy demands of this project. Even with the fast technical evolution in this field, state-of-the-art digital cameras still do not provide the image dimensions and the excellent image quality produced by the SMK 40 – especially they lack its stable geometry. However, suitable cameras are bound to enter the market, since CCD chips holding 2k x 2k pixels (Luhmann 1991) and cameras with pixel synchronization for stable image geometry like the VIDEK MegaPlus are already available, though still not featuring the needed pixel resolution. Back in 1986/7 when concepts for the project were made, a rapid development like this had not been foreseen.

However, possible advantages of digital image acquisition for close range applications were to be researched, and for this purpose an experimental digital stereo-image acquisition system (DigiSAS) was designed at the TU Berlin. This system became operational during the project work but, due to hardware limitations, was used only for testing purposes. It is able to capture images from two CCD cameras with 512 x 512 pixels (8 bit) each, simultaneously using external line synchronization (Jeschke 1990). Thus only a poor accuracy of several mm for the project test areas was possible, which was not appropriate for precise surface measurements. Nevertheless some valuable experiences in handling of digital cameras for close range applications were made during the practical tests of DigiSAS. Using non-photogrammetric cameras brings up the problem of calibration. Image orientation is also more complicated – compared to the SMK with its fixed base and camera directions – and reference points are needed, the more the better.

For the DigiSAS tests a 3-D metal frame holding some 20 reference points was built. Several test series were done, checking geometrical stability and the possible accuracy of the system. During these tests the influence of often reported (Beyer 1987, Daehler 1987, Lenz & Fritsch 1988) problems like line-jitter, aliasing, and warm-up effects on image quality and evaluation results

were measured. Effects on geometric image quality were up to 2 pixels and, still worse, image distorsions appeared to be randomly distributed and unpredictable. Thus a system calibration in advance of the practical tests was impossible. Instead, the camera's distortion parameters had to be measured during the actual image acquisition. This was done using the calibration frame mentioned above, shooting images of the frame immediately before and after the actual images to be evaluated. The two calibration results yielded by bundle-block adjustment subsequently were interpolated. This method may be applicable for all kinds of non-photogrammetric cameras, especially unstable digital cameras with rather fast changing distortion parameters, reducing the work for measuring reference points in the field. Of course, the calibration object itself must be reliable and stable enough for this task. If rough starting values for the orientation parameters can be provided, targets on the frame can be measured automatically in digital images since their object coordinates are known. This method worked with DigiSAS images and can ease tedious orientation measurements with their many image coordinates to be registered.

IMAGE EVALUATION

Orientation and Image Matching

These are standard tasks of digital photogrammetry. At the TU Berlin the Digital Stereophotogrammetric System (DSS) generally is used to do the interior, relative, and absolute orientation as well as to resample the images to the normal case of sterophotogrammetry and, finally, to match them automatically in a multistep process (KÖNIG ET AL. 1988). However, since almost all 'real work' in this project was done with images of a properly calibrated SMK, the actual orientation process was still easier and consisted of an affine transformation of each image with respect to the fiducial marks and a simple rotation/translation to consider offset and tilt caused by the scanning process. After that, the data are ready for image matching, i.e. determination of homologous image points.

A combination of normalized cross-correlation and least-squares matching is used. Since the latter needs good starting values, an image pyramid strategy is used starting at the level of lowest resolution with a one-dimensional cross correlation process that works without operator assistance. Correlation results are considered approximate values in the next pyramid level which makes matching a totally automatic process. On each level the point raster is densified until the bottom level is reached. In order to keep computation time short, only in this original image the least-squares method is used to provide sub-pixel results. The found matches undergo a quality control, where several criteria are tested and it is decided which results are accepted. Recently, the two steps that consume the lion's share of computation time, i.e. resampling and matching, are sped up considerably by the mutation of the DSS into an Advanced DSS (ALBERTZ ET AL. 1991, ALBERTZ & KÖNIG 1991). In the actual constellation this system uses a 14-transputer Paracom MultiCluster hosted on a SUN workstation.

DEM COMPUTATION

After the image matching process the parallax file defining homologous points in the stereo images has to be transformed into object coordinates. The resulting 3D coordinates are related to the selected geodetic reference system. The rectangular metal frames around the soil test areas were used to define a system with a reference point in the lower left corner (as seen in the images). This coordinate system allowed the comparison of multitemporal images and resulting DEMs, which was the main objective of the measurements. Before interpolating a regularly gridded DEM, application of a filter for the elimination of blunders in the height points proved to be useful. This filter contained two components. First, minimal/maximal threshholds for Z-coordinates (heights) and second, a statistical elimination of local peaks with extraordinary height differences in comparison to their surrounding points. It was especially designed to eliminate blunders which could have a negative effect during the following interpolation process.

Advantageous for graphical representations as well as for further numerical analysis is a regular grid of heights. Several algorithms have been tested with examples of different relief models, i.e. sharp edges, holes and crests. The influence of the height point distribution on the interpolation results was examined because a dense regular distribution that guarantees the best results possible often can not be achieved. A good interpolation algorithm has to be robust concerning gaps in the distribution which may originate from correlation errors eliminated by the previous filtering or from shadow zones where no correlation is possible. The following interpolation methods were compared: nearest neighbourhood, minimum curvature, polynomial interpolation, and finite elements (HIFI-88).

During tests the minimum curvature algorithm (BRIGGS 1974) proved to be the most suitable method under given circumstances. HIFI-88 did not perform that well. However, it was designed to use additional information (e.g. break lines) in the interpolation process that our evaluation process did not provide. Polynomial interpolation worked well as long as the height points were densely and regularly distributed, otherwise it had problems. Nearest neighbourhood is suitable only for rough reliefs with measured points distributed more densely than the grid points wanted in the end. The resulting regular DEM could be processed further by various methods in order to identify and eliminate blunders that may have passed all previous tests. The last step is the interactive control and – if necessary – correction of the DEM which can be displayed in isolines, as a 3D wireframe model and so on. For special comparison purposes the extraction of height profiles was implemented and differential DEMs can be computed to capture relief changes.

SUBSEQUENT PROCESSING OF DEM RESULTS

DEMs for further processing were available with the parameters listed in table 1. A five point margin was cut from the models to eliminate marginal effects that might be caused by the surrounding frame, thus resulting in 45,600 elevation points on 0.182 m^2 in the laboratory models (and 102,400 from 0.92 m^2 in the field models). For each microrelief two characteristic values were computed, i.e. the indices *RRC* (random roughness coefficient, according to CURRENCE & LOVELY 1970) and the ratio *TSA/MA* (total surface area to map area, this helps providing a quantitative measure for the raindrop density).

Parameter	Laboratory	Field
Area of measurement	0.2 m^2	0.98 m^2
Spacing	2 mm	3 mm
Height resolution	0.2 mm	0.2 mm
Number of data	50,000	108,900

Table 1: Parameters for microrelief measurement

RRC represents the variance of the smoothed height values. Smoothing results in elimination of external relief effects like slope and directional relief elements. TSA/MA was computed as ratio of the sum of all surface areas of the DEM (there are 45,171 resp. 101,761 raster squares) divided by the DEM ground area (i.e. the TSA mapped on the ground). For the registration of spatial structures in the microreliefs semivariograms were computed. These data were smoothed too, in order to get out trends and the low-frequency variance caused by slope.

DETERMINISTIC MODELS

Effective input of rainfall energy

For calculation of the effective rainfall energy that hits the soil surface, the total surface area (explained above) and as well the normal component of rainfall energy, depending on the angle of drop impact, is needed. This parameter is computed by determining the slope of the soil surface in each grid square of 4 mm^2 for lab and 9 mm^2 for field plots. Assuming vertical rainfall and a horizontal soil surface, the normal component of the impact energy corresponds to the total kinetic energy. With increasing slope at the striking point the normal component decreases with respect to the impact vector, leading to a decrease in effective energy. The normal component thus is proportional to the cosine of the slope at the impact point (fig. 2).

Effective input of kinetic rain energy with respect to TSA and amount of rainfall may be expressed as:

$$E.eff = ma/tsa * \sum (\cos \alpha * E.kin) \quad (1)$$

α = soil surface slope; ma = map area (m^2); tsa = total surface area (m^2)

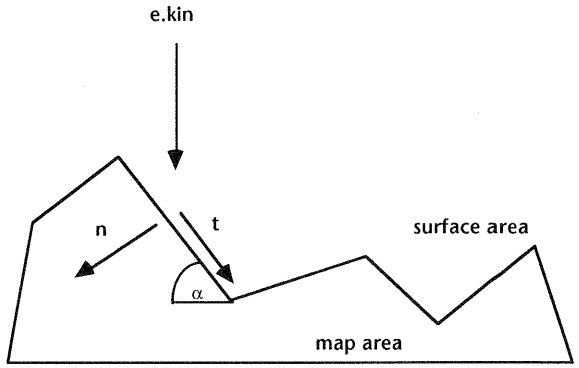

Fig. 2: Relation between surface slope, impact angle and the distribution of impact force

α = slope angle, E.kin = kinetic energy of raindrop, n = normal component of impact force, t = tangential component of impact force

Depressional storage

Storage capacity was determined by finding each depression in the relief and estimating its circumference, surface area and volume. Identification of a depression was carried out starting from the *pour point,* defined as the lowest point between two or more depressions and within an elevated area. With the pour point as basis, closed contour lines were determined that laid either at the same or at a lower height than that of the pour point. The area within such a contour line was defined as a depression. Thus the extent of a depression is equal to the length of the respective contour line. The vertical distance between the lowest point and the pour point is the maximum filling height. The surface area was calculated using vector geometrics the same way as for the TSA. Elevated areas within a depression (islands) were subtracted. This technique of finding depressions complies with the theory proposed by ULLAH & DICKINSON (1979) and HUANG & BRADFORD (1990B). However, they began from a local depression and identified the pour point by checking the list of neighboring points until finding a point with a lower elevation. This leads to more or less rectangular depression forms. The procedure proposed here has the advantage, that the whole depression is characterized independently of its form.

RESULTS AND DISCUSSION

Microrelief characterization

The microrelief parameters obtained from the DEMs are summarized in table 2.

In all cases, rainfall lowers the TSA/MA ratio by about 0.1. Thus, the total surface area of the three microrelief treatments differs significantly and the relative change caused by rainfall is slightly greater for the fine microrelief. In the field experiments the ratio of TSA/MA for both sites showed values that were comparable to that from the lab. Thus, the laboratory simulations seem to be representative of natural conditions as measured in

		Laboratory			Field		
Treatment		f	m	r		site 1	site 2
tsa/ma							
relation between	before and	1.12	1.27	1.44	1st date	1.34	1.22
total surface area	after rain	1.02	1.14	1.37	2nd date	1.23	1.13
and map area							
RRC							
Index according	before and	2.3	4.3	8.5	1st date	7.7	5.3
to *Currence and*	after rain	1.4	3.2	7.5	2nd date	7.0	4.0
Lovely (1970)							

Table 2: Indices from microrelief describing DEMs

the field. An increase in the microrelief roughness doubled the value for RRC. The microrelief differences are well characterized by this index. For the field experiments the decrease of RRC due to rainfall was minor than but still comparable to that of the laboratory treatments. Thus both indices seem to be capable to characterize microrelief and changes due to rainfall in the field as well as in the laboratory.

Semivariograms were calculated in order to identify possible spatial patterns. Figs. 3a and 3b show semivariograms for the rough and fine surfaces, each before and after rainfall. In the beginning all curves show a sharp rise with the lag, until a sill is reached at greater lag values. The range within which a spatial dependence of the investigated parameter is visible, is marked by arrows in the figures. For the rough surface, the range corresponds to a lag h of 25, while the range is about 12 to 14 in the medium treatment, not shown here. These lag values are equivalent to 50 mm and 25 mm, respectively (1 h = 2 mm). This corresponds to the openings of the sieves that were used to fill in the soil material and depicts the maximum diameters of the largest aggregates or clods in each microrelief type. After rainfall range tended to increase slightly, which might be due to a relative flattening of the bigger clods. Thus, with the help of semivariograms, it is possible to confirm the importance of big clods as surface shaping elements. For the fine treatment there is no clearly identifiable sill, just a lowered gradient in the range of 7 to 10. In this case there is no reliable identification of the largest clods (10 mm diameter) since this is just four times the height value spacing and within this comparably high-frequent range no characteristic sill is possible. The sills in the semivariograms are significantly different. Rainfall led to a relative reduction of the sill by about 20% for the rough, 50% for the medium, and 25% for the fine treatment, respectively. The absence of *nugget variance* in all semivariograms indicates that the grid distance is small enough to fully characterize the variation in surface microrelief. Higher resolution in microrelief variation would not yield any further information. Results of the semivariograms from the field experiment DEMs were similar to those of the medium treatment above. Here nugget variance was missing, too.

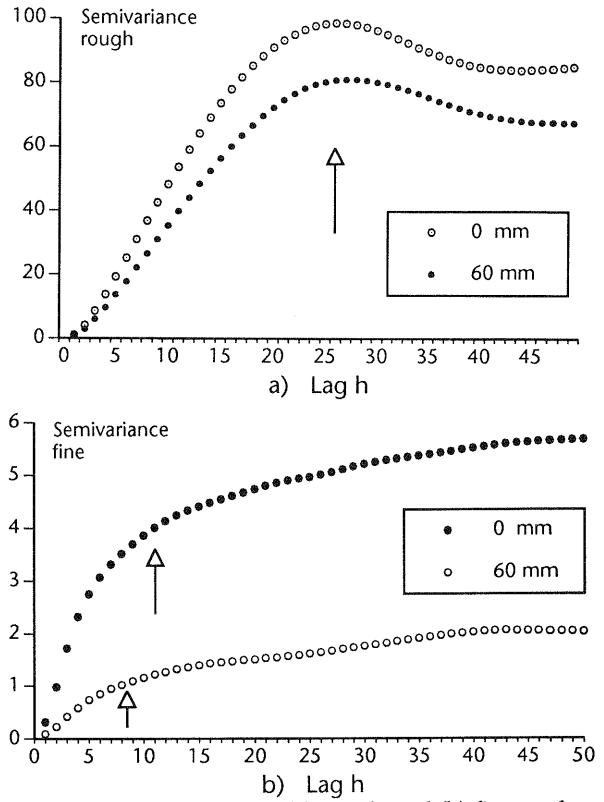

Fig. 3: Semivariograms for (a) rough and (b) fine surfaces before and after rainfall (lag h = 2 mm).

Energy dissipation

The kinetic energy of raindrops impinging on the soil surface leads to surface sealing, which is the actual trigger mechanism for runoff formation. As discussed earlier, the TSA/MA ratio affects the total input of rainfall energy. The effective normal component of impact force with respect to impact angle is also relevant to splash detachment and thus to sealing. Table 3 shows the calculated effective energy (the normal component of impact force with respect to the TSA) in percent of the kinetic energy as simulated in the laboratory experiments.

	Laboratory			Field	
Treatment	f	m	r	site 1	site 2
E.eff (%)					
before and	84	65	56	1st date	62	71
after rain	95	80	67	2nd date	71	82

Table 3: effective rainfall energy E.eff (J/m^2 tsa) in percent of the kinetic rainfall energy (J/m^2 ma)

The effective rainfall energy for the rough treatments is only about one half of its kinetic energy. This share is significantly larger for the medium and fine areas. Even after the rain there is considerable energy reduction in the rough and medium areas. To verify the theory that the microrelief induced effective rain energy substantially influences silting and surface runoff, we must compare the runoff measured in the laboratory with the effective rain energy. Figures 4a and 4b show runoff curves. In fig. 4a the cumulated runoff is plotted against cumulated kinetic energy as it is usual in literature.

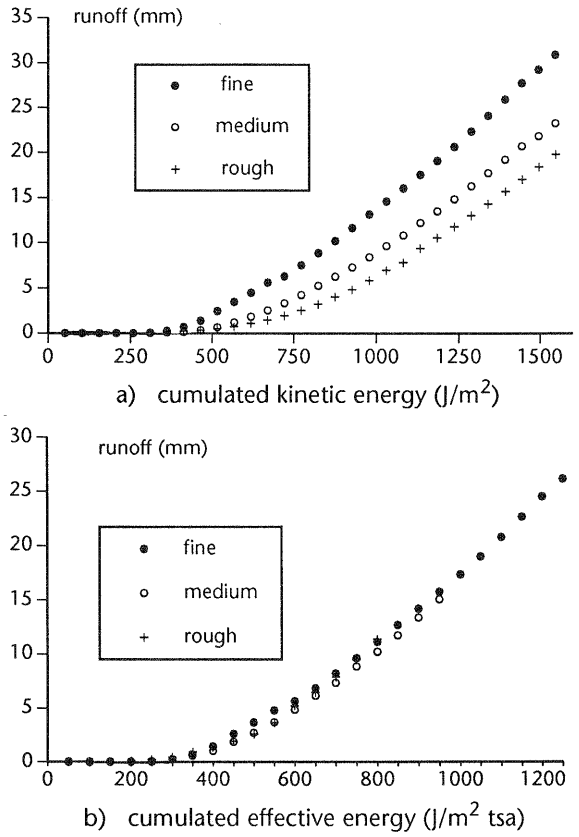

Fig. 4: Results of runoff measurements obtained from the rainfall simulator. Total runoff is shown as function of cumulated (a) kinetic and (b) effective rainfall energy

Fig. 4b shows cumulated runoff plotted against cumulated effective energy as calculated from the DEMs. Differences in total runoff are up to 60% between rough and fine treatment, respectively. When plotted against microrelief dependent effective energy, runoff curves now coalesce, showing that microrelief effects on runoff depend in fact on variations in effective energy input. This implies the verification of this theory for the first time.

Depressional storage

The calculated depressional storage of rainfall, number of depressions, surface area, depths and extent is summarized in table 4. Before rain, the runoff plots from the laboratory contained about 15 to 36 depressions. Field plots had significantly more depressions. From the total volume, a storage capacity of less than 0.3 mm rain for a rough microrelief can be computed (there are two reasons leading to less depressional storage with a finer microrelief: less depressions and less extent of depressions).

Considering these figures none of the surfaces is able to decisively delay the beginning of runoff. Even a storage capacity of 1.2 mm just gives a runoff delay of 2 minutes when rained with an intensity of 30 mm/h. Moreover, the relative area of the depressions decreases with the rainfall which leaves only a minimal storage capacity at the end of rainfall. From these results it becomes evident that – contrary to the hypothesis commonly proposed – depressional storage does not necessarily have a great influence on runoff. Other authors have reported significantly larger storage capacities (LINDEN & VAN DOREN 1986). However, their calculations mainly referred to microreliefs resulting from primary tillage and were based on relief data that did not allow for such exact determinations (they used for instance grid distances of 20-50 mm. Only ULLAH & DICKINSON (1979), and HUANG & BRADFORD (1990b) came to values of up to 2 mm. As both the grid distance and the method of defining depressions used by the latter authors was similar to the technique used here, it seems justified to state that microrelief dependent depressional storage does not have a significant impact on runoff delay.

	Laboratory			Field	
Treatment	f	m	r	site 1	site 2
depressional storage (mm)					
before and	0.01	0.08	0.34	1st date	1.2	0.1
after rain	0	0.01	0.03	2nd date	0.09	0.06
surface area Σ (%)					
before and	3	6	13	1st date	13	7
after rain	0.2	1	2	2nd date	5	4
depth (mm)					
before and	1.8	2.4	2.9	1st date	2.2	2.0
after rain	1.2	1.5	1.6	2nd date	1.6	1.6
extent (mm)					
before and	50	55	62	1st date	62	70
after rain	39	67	41	2nd date	46	64
number					
before and	15	36	32	1st date	225	71
after rain	7	12	16	2nd date	25	65

Table 4: Depressional storage, volume per 0.18 m² (mm of rainfall), surface area in percent of total surface area, number of depressions per 0.18 m², median of depth, and median of extent.

CONCLUSIONS

This project demonstrated that close-range photogrammetry combined with digital image evaluation is a suitable method for surface measurement of soil. Digital image matching for DEM computation has come a long way and is widely used and acknowledged. Computation times have rapidly decreased due to hardware improvements and automated measurement of image coordinates for large numbers of points can be done in acceptable time. The photogrammetric techniques allow to obtain microrelief data with sufficient resolution in order to derive various statistical and geostatistical indices describing the microrelief. Specifically, the method enables an accurate calculation of depressional storage (even just to show it does not play such an important role) and effective input of rainfall energy. Both parameters are essential for understanding the interactions between rainfall, surface sealing, and runoff formation. Methodical improvements may come from edge correlation (able to provide just that kind of information which can not be won by the area-based matching methods (LI 1990). Since digital image acquisition using CCD cameras is almost operational, it soon will be possible to profit from direct digital image re-

cording. Conventional photogrammetric cameras will become obsolete for most purposes.

However, as long as image processing and matching requires a considerable amount of computation time the use of this method for routine measurements is questionable. At least for the near future laser reliefmeters, using a contact-free and non-destructive method as well, promise to deliver data of the same type in shorter time. These systems may become serious competition for photogrammetry. But since they are subject to certain restrictions their main advantage, the direct measurement of a regular DEM in a substantially shorter time, has to be weighted against the possibility of allowing measurement and interpretation based on the very same images. Furthermore, scanning systems need always longer time to cover a predefined area than it takes shooting a photograph (making them useless for moving objects). Close-range photogrammetry still has its advantages (and, hopefully, lots of other application fields), which should be developed in the future using the technical evolution.

ACKNOWLEDGEMENTS

The major part of this work has been supported by the Technical University of Berlin through the Interdisciplinary Research Project 'Measurement and Interpretation of Surfaces'. The efforts of Christian H. Roth and others at the Institute for Ecology at the Technical University of Berlin (rain simulator, testing) and of Rainer Wolf (software) are greatfully acknowledged.

REFERENCES

ALBERTZ, J., W. JESCHKE, G. KÖNIG, J. STORL AND F. WEWEL, 1991. Transputer-Netzwerke und ihr Einsatz in Digitalen Photogrammetrischen Systemen. Z. Photogramm. Fernerk. 59: 65-73.

ALBERTZ, J. AND G. KÖNIG, 1991. The Advanced Digital Stereophotogrammetric System of the TU Berlin. Digital Photogrammetric Systems, eds. H. Ebner, D. Fritsch and C. Heipke, Wichmann, Karlsruhe: 17-27.

BEYER, H.A., 1987. Some aspects of the geometric calibration of CCD cameras. ISPRS Intercomm. Conf. Interlaken: 68-81.

BRIGGS, I.C., 1974. Machine contouring using minimum curvature. Geophysics 39: 39-48.

BURWELL, R.E., R.R. ALLMARAS, AND M. AMEMEIYA, 1963. A field measurement of total porosity and surface microrelief of soils. Soil Sci. Am. Proc. 27: 697-700.

CURRENCE, H.D. AND W.G. LOVELY, 1970. The analysis of soil surface roughness. Trans ASAE 13: 710-714.

DAEHLER, J., 1987. Problems in digital image acquisition with CCD cameras. ISPRS Intercomm. Conf. Interlaken: 48-59.

FERREIRA, A.G. AND M.J. SINGER, 1985. Energy dissipation of waterdrop impact into shallow pools. Soil Sci. Soc. Am. J. 49: 1537-1541.

HUANG, C. AND J.M. BRADFORD, 1990A. Portable laser scanner for measuring soil surface roughness. Soil Sci. Soc. Am. J. 54: 1402-1406.

HUANG, C. AND J.M. BRADFORD, 1990B. Depressional storage for markov-gaussian surfaces. Water Resources Res. 26: 2235-2242.

JESCHKE, W., 1990. Digital close-range photogrammetry for surface measurement. SPIE 1395 (Int. Arch. Photogramm. Rem. Sens. 28(5)): 1058-1065.

JOHNSON, C.B., J.V. MANNERING AND W.C. MOLDENHAUER, 1979. Influence of surface roughness and clod size on soil and water loss. Soil Sci. Soc. Am. J. 43: 772-777.

KÖNIG, G., W. NICKEL AND J. STORL, 1988. Digital Stereophotogrammetry – Experience with an experimental System. Int. Arch. Photogramm. Rem. Sens. 27(B2): 326-331.

LENZ, R. AND D. FRITSCH, 1988. On the accuracy of Videometry. Int. Arch. Phot. Rem. Sens. 27(B5): 335-345.

LI, R., 1990. Erfassung unstetiger Oberflächen aus digitalen Bilddaten durch Flächen- und Kantenzuordnung. DGK, C 364, Munich.

LINDEN, D.R. AND D.M. VAN DOREN, 1986. Parameters for characterization tillage induced soil surface roughness. Soil Sci. Soc. Am. J. 50: 1560-1565.

LINDEN, D.R., D.M. VAN DOREN AND R.R. ALLMARAS, 1988. A model of the effect of tillage induced soil surface roughness on erosion. Int Soil Tillage Res. Org., 11th Int. Conf. on Tillage and Traffic in Crop Production 1: 373-378.

LUHMANN, T., 1991. Aufnahmesysteme für die Nahbereichsphotogrammetrie. Z. Photogramm. Fernerk. 59: 80-87.

MOORE, I.D. AND C.L. LARSON, 1979. Estimating microrelief surface storage from point data. Trans ASAE 22: 1073-1077.

RÖMKENS, M.J.M. AND J.Y. WANG 1984. The effect of tillage on surface roughness. ASAE Paper 84: 2026.

ROTH, C.H. AND K. HELMING, 1992. Dynamics of surface sealing, runoff formation, and interrill soil loss as related to rainfall intensity, microrelief, and slope. Z. Pflanzenernähr. Bodenk. 56 (in press).

STEICHEN, J.M., 1984. Infiltration and random roughness of a tilled and untilled claypan soil. Soil and Tillage Research 4: 251-262.

TESSIER, S., R.I. PAPENDICK, K.E. SAXTON AND G.M. HYDE, 1989. Roughness meter to measure seed row geometry and soil distubance. Trans ASAE 32: 1871-1873.

ULLAH, W. AND W.T. DICKINSON, 1979. Quantitative description of depression storage using a digital surface model, I. deterination of depression storage, II. characteristics of surface depressions. J. of Hydrology 42: 63-90.